IEEE Photonics Journal
An IEEE Photonics Society Publication

Open Access

Spatial Quantum Beating of Adjustable Biphoton Frequency Comb With High-Dimensional Frequency-Bin Entanglement

Volume 11, Number 4, August 2019

Rong Xue
Xin Yao
Xu Liu
Heqing Wang
Hao Li
Zhen Wang
Lixing You
Yidong Huang
Wei Zhang

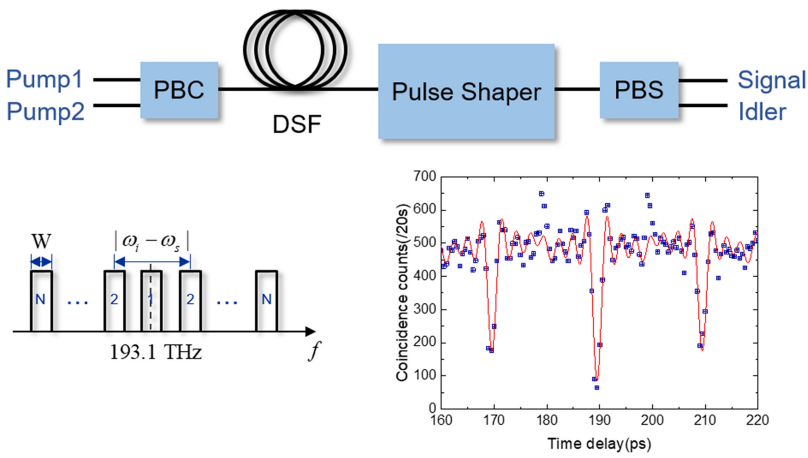

DOI: 10.1109/JPHOT.2019.2922282
1943-0655 © 2019 IEEE

Spatial Quantum Beating of Adjustable Biphoton Frequency Comb With High-Dimensional Frequency-Bin Entanglement

Rong Xue,[1,2] **Xin Yao**,[1,2] **Xu Liu**,[1,2] **Heqing Wang**,[3] **Hao Li**,[3] **Zhen Wang**,[3] **Lixing You**,[3] **Yidong Huang**,[1,2] **and Wei Zhang** [1,2]

[1]Beijing National Research Center for Information Science and Technology, Beijing Innovation Center for Future Chips, Electronic Engineering Department, Tsinghua University, Beijing 100084, China
[2]Beijing Academy of Quantum Information Sciences, Beijing 100193, China
[3]State Key Laboratory of Functional Materials for Informatics, Shanghai Institute of Microsystem and Information Technology, Chinese Academy of Sciences, Shanghai 200050, China

DOI:10.1109/JPHOT.2019.2922282

Manuscript received April 15, 2019; revised May 31, 2019; accepted June 7, 2019. Date of publication July 12, 2019; date of current version July 26, 2019. This work was supported in part by the National Key R&D Program of China under Contract 2017YFA0303704 and 2017YFA0304000, in part by the National Natural Science Foundation of China under Contract 61575102, 91750206, 61671438, 61875101, and 61621064, in part by the Beijing National Science Foundation under Contract Z180012, and in part by Beijing Academy of Quantum Information Sciences under Contract Y18G26. Corresponding author: Wei Zhang (e-mail: zwei@tsinghua.edu.cn).

Abstract: In this paper, we realize an adjustable biphoton frequency comb and investigate its spatial quantum beating. Vector spontaneous four wave mixing processes in a piece of dispersion shifted fiber are produced by non-degenerate continuous wave pump lights with orthogonal polarizations to generate broadband biphoton states, and then a pulse shaper is used to realize the biphoton frequency comb with high-dimensional frequency-bin entanglement. The property of the biphoton frequency comb is indicated by the shape of the fringes of spatial quantum beating, which is also comb-like with a series of dips. The variations of the beating fringes show the changes of frequency bins in the comb by the setting of the pulse shaper. It can be expected that the adjustable biphoton frequency comb has great potential on high-dimensional quantum information processing and quantum communication based on the frequency degree of freedom.

Index Terms: Fiber nonlinear optics, quantum entanglement, spatial quantum beating.

1. Introduction

High-dimensional entanglement is a crucial resource for quantum communication [1], [2], quantum information [3], [4], and quantum computation [5]. Recently, high-dimensional frequency-bin entangled biphoton states attract much attention. On one hand, with the development of state transformation techniques in frequency domain [3], [6]–[8], they have shown important potential in high-dimensional quantum information processing. On the other hand, they are also widely used in quantum metrology based on quantum interferometry [9].

High-dimensional frequency-bin entangled biphoton states can be generated by either spontaneous parametric down conversion (SPDC) [6], [10] or spontaneous four wave mixing (SFWM) [3], utilizing the filtering effect of optical resonators. They are also known as quantum optical frequency combs [11]–[13]. First, the broadband biphoton state with time-energy entanglement is generated by SPDC or SFWM in a nonlinear medium. Then it is filtered by an optical resonator to get the biphoton frequency comb with frequency-bin entanglement [6], [14]. The nonlinear medium also could be placed into the resonator [15], by which the pump light and the nonlinear interaction are enhanced to improve the brightness of the biphoton frequency comb. The property of biphoton frequency comb can be indicated by the experiment of spatial quantum beating [16]–[20]. The fringes of spatial quantum beating can be explained by the interference between the photons output from the resonators after different round-trip time. Hence, the spatial quantum beating pattern are highly determined by the resonator, which also determines the frequency bins of the biphoton frequency comb.

Recently, programmable optical filters based on spatial dispersion components and spatial light modulators have developed rapidly [21], named as pulse shapers. They can make flexible control of amplitudes, phases, group delays and dispersions over a broad frequency range with high frequency resolution, and have been used in shaping of ultrafast optical pulses, optical signal processing of microwave photonics and so on [22], [23]. In this paper, we apply a pulse shaper to realize adjustable biphoton frequency comb by vector SFWM in a piece of fiber and investigate its spatial quantum beating. The property of the biphoton frequency comb is indicated by the shape of the beating fringes. The variations of the beating fringes show the tuning of the comb by changing the parameter setting of the pulse shaper. The experiment results show that the biphoton frequency comb can be flexibly adjusted by the pulse shaper and is convenient in researches of high-dimensional quantum information applications.

2. Adjustable Biphoton Frequency Comb and Its Spatial Quantum Beating

SFWM is a type of third-order nonlinear process, in which two pump photons are annihilated while a photon pair is generated simultaneously. Usually the photon with higher frequency of the pair is named as signal photon, and the photon with lower frequency is named as idler photon. The SFWM process satisfies the energy conservation, which is expressed as

$$\omega_{p1} + \omega_{p2} = \omega_s + \omega_i \tag{1}$$

where ω_{p1} and ω_{p2} denote the frequencies of two pump photons, ω_{s} and ω_{i} denote the frequencies of the signal photon and the idler photon, respectively. It also satisfies the momentum conservation, which is in the form of phase-matching condition of four wave mixing and determines the bandwidth of the generated biphoton state. If the annihilated pump photons have the same polarization, and the generated signal and idler photons are also in this polarization, the process is named as scalar SFWM. Besides, if the two pump photons are in orthogonal polarizations, and the generated signal and idler photons are also orthogonally polarized, the process is named as vector SFWM [24]–[26].

In this work, the biphoton frequency comb with high-dimensional frequency-bin entanglement is realized by vector SFWM under non-degenerate pumping in a piece of dispersion shifted fiber (DSF), as illustrated in Fig. 1(a). Two continuous wave (CW) pump lights with different frequencies and orthogonal polarizations are injected into the DSF, leading to two vector SFWM processes simultaneously. In one process, the signal photon is in horizontal polarization (H) while the idler photon is in vertical polarization (V), as shown in Fig. 1(b). In the other process, the signal photon is in V while the idler photon is in H, as shown in Fig. 1(c). The two processes are indistinguishable and coherently superposed, generating the biphoton state with hyper-entanglement [26]. And then it is filtered by a pulse shaper to realize the biphoton frequency comb, as shown in Fig. 1(d). Parameters of the comb can be tuned by the pulse shaper. Finally, the two photons in one pair are separated into two ports by a polarization beam splitter (PBS), and the frequency of the generated photons in

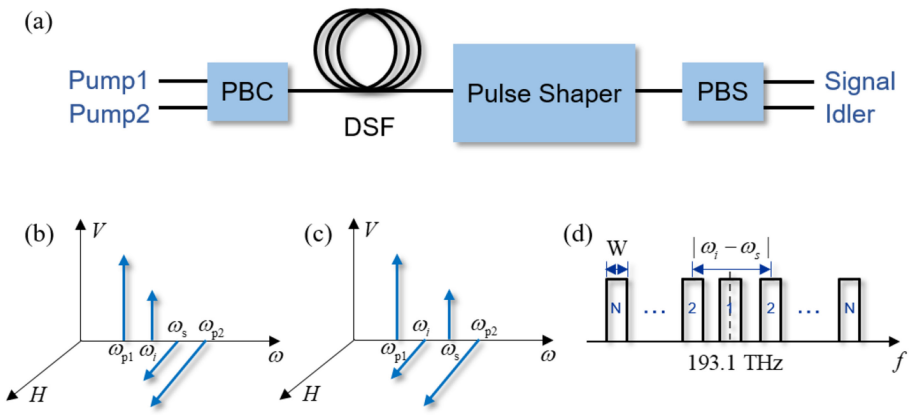

Fig. 1. (a) Scheme of the biphoton frequency comb generation. PBC, polarization beam combiner; DSF, dispersion shifted fiber; PBS, polarization beam splitter. (b) and (c) Two indistinguishable vector SFWM processes. (d) The biphoton frequency comb controlled by the pulse shaper.

each port is uncertain. The state of the biphoton frequency comb can be expressed as

$$|\psi_N>=\frac{1}{\sqrt{2N}}\sum_{n=1}^{N}(|\omega_{in}\omega_{sn}>+|\omega_{sn}\omega_{in}>) \tag{2}$$

showing the property of high-dimensional frequency-bin entanglement. In above expression, ω_{sn} and ω_{in} are signal and idler frequencies of a pair of the frequency comb satisfying Eq. (1). N is the total number of the frequency comb pairs in the biphoton state and n is the label of a specific frequency comb pair.

The property of the biphoton frequency comb can be indicated by the spatial quantum beating experiment [16]. In the experiment, the two photons entangled in frequency are injected into a 50:50 fiber coupler with a controlled arrival time delay, and then detected by single photon detectors, respectively. The coincidence counts of the detectors under different photon arrival time show the fringes of spatial quantum beating. For the biphoton state with one frequency comb pair (N = 1 in Eq. (2)), the normalized coincidence counts of spatial quantum beating can be expressed as [16]

$$\begin{aligned} N_{c_1} &\propto 1 - Vf(\tau)\cos(|\omega_i - \omega_s|\tau) \\ &= 1 - V\mathrm{sinc}(W\tau)\cos(|\omega_i - \omega_s|\tau) \end{aligned} \tag{3}$$

where V is the fringe visibility of spatial quantum beating, τ is the time delay between the signal and idler photons, $|\omega_i - \omega_s|$ is the frequency difference between the signal and idler photons, $f(\tau)$ is a time-domain function obtained by inverse Fourier transform of the spectra of signal and idler photons. Considering that the filtering profile of the pulse shaper can be regarded as a rectangle function with a bandwidth of W, the corresponding $f(\tau)$ can be written as $\mathrm{sinc}(W\tau)$. It can be seen that $f(\tau)$ determines the envelope and $\cos(|\omega_i - \omega_s|)$ determines the period of the fringes.

For the biphoton frequency comb with multi-comb pairs (N > 1 in Eq. (2)), the spatial quantum beating shows different fringe profiles. According to the generation process of this biphoton state, it can be seen that a specific photon pair will appear in a specific frequency comb pair. Hence, the fringe profile of this state can be constructed by superposing fringes of different frequency comb pairs. The corresponding normalized coincidence counts can be expressed as

$$N_{c_N} \propto \sum_{n=1}^{N}[1 - V_n f_n(\tau)\cos(|\omega_{in} - \omega_{sn}|\tau)] \tag{4}$$

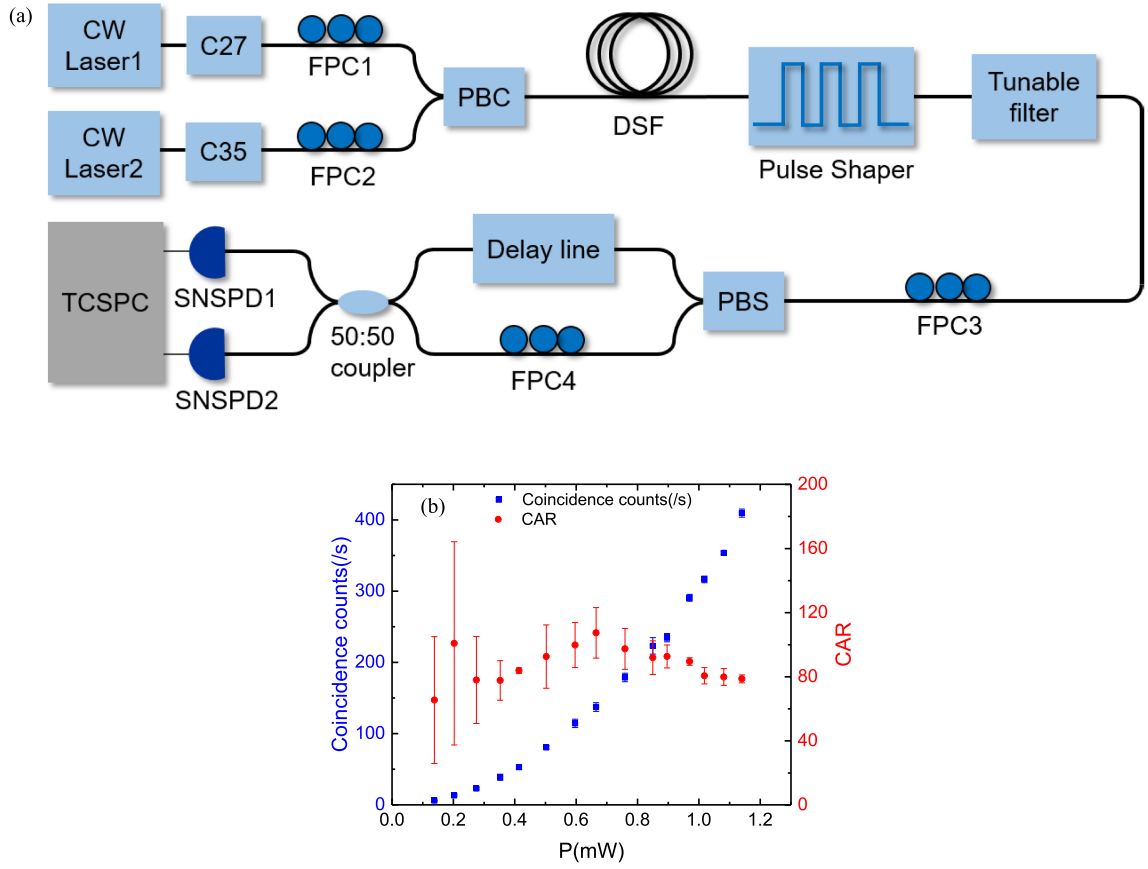

Fig. 2. (a) Experiment setup for the spatial quantum beating. C27 and C35, dense wavelength division multiplexer modules; FPC, fiber polarization controller; PBC, polarization beam combiner; DSF, dispersion shifted fiber; Tunable filter, bandwidth-variable tunable filter; PBS, polarization beam splitter; SNSPD, superconducting nanowire single photon detector; TCSPC, time correlated single photon counting module. (b) Coincidence count rates (blue) and CARs (red) of the fiber based biphoton source under different pump levels.

If all the frequency comb components have the same rectangle spectral profile with the bandwidth of W and the visibility of V, Eq. (4) can be written as

$$N_{c_N} \propto N - V\mathrm{sinc}(W\tau)\sum_{n=1}^{N}\cos(|\omega_{in} - \omega_{sn}|\tau) \tag{5}$$

It can be seen that f(τ) still determines the whole envelop of the fringes, however, the fringes are determined by the sum of a series of cosine functions. If the frequency comb pairs are selected by the pulse shaper with equal frequency comb spacing, it can be expected that the fringes would also be comb-like, showing a series of dips like the pulse formation of mode locked lasers in time domain.

3. Experiment and Results

The experiment setup for the spatial quantum beating of the biphoton frequency comb is shown in Fig. 2(a). Two CW lasers are utilized as pump lights with central wavelengths of 1549.315 nm (C35, ITU channel 35) and 1555.74 nm (C27, ITU channel 27), respectively. Both of them have an output power of 20 mW. The two pump lights pass through the optical filter modules (DWDM C27 and C35 for CW laser1 and 2, respectively) to suppress noise photons at the signal and idler frequencies.

Then they are combined by a polarization beam combiner (PBC) under orthogonal polarizations and injected into a piece of DSF to produce vector SFWM processes. The fiber polarization controllers (FPC1, FPC2) before the PBC are used to adjust the polarization direction of the pump lights. The 250-meter-long DSF is cooled in the same cryostat with superconducting nanowire single photon detectors (SNSPDs) to suppress the noise photons generated by the spontaneous Raman scattering [27]. A pulse shaper (Waveshaper 1000A, Finisar Inc.) is used to select signal and idler photon pairs of the biphoton frequency comb. The bandwidth-variable tunable filter is then cascaded to further filter out the residual pump lights. And the generated photons are separated by a PBS. The FPC3 before the PBS is used to adjust the polarizations of the generated photons, ensuring that the photon pairs at the two ports of PBS are in the high-dimensional frequency-bin entangled states, as shown in Eq. (2).

Firstly, one frequency comb pair is selected by the pulse shaper to evaluate the performance of the source, and the results are shown in Fig. 2(b). In the measurement, both signal and idler photons have a rectangle spectral profile, with respective central frequency of 193.0 THz and 193.2 THz, and bandwidth of 100 GHz. The photons are directly detected at the output ports of the PBS by two SNSPDs (Fabricated by SIMIT, China) [28]. The detection efficiencies and dark-count rates of the two SNSPDs are $\sim$50% at 1550 nm and $\sim$200 Hz, respectively. The detection events of the SNSPDs are recorded by the time correlated single photon counting module (TCSPC, PicoQuant, HydraHarp 400). Fig. 2(b) shows the coincidence count rates and the ratio of coincidence counts to accidental coincidence counts (CAR) under different pump levels, which indicates the noise characteristic of the biphoton source [29]. The pump levels are monitored by a 90:10 fiber coupler followed by the PBC, which is not shown in Fig. 2(a). It can be seen that the CAR is more than 80 when the pump level is around 1 mW, under which the coincidence count rate is more than 300 Hz. The results indicate that the fiber based biphoton source has a good noise characteristic under a high photon pair generation rate.

Fig. 3 shows the measurement results of spatial quantum beating of the generated photon pairs. In the measurement, the photons output from the two ports of the PBS are injected into a 50:50 fiber coupler, as shown in Fig. 2(a). The variable delay line (VDL) at one input port of the fiber coupler is used to adjust the arrival time of the photons at this port, and the FPC4 at the other input port of the fiber coupler is used to ensure that the photons at the two input ports have the same polarization. The data points in Fig. 3 are coincidence counts without subtraction of accidental coincidence counts under different delay time of the VDL, and the solid line is the fitting curve. Fig. 3(a) are the results when the signal and idler photons have the same rectangle spectral profile with a central frequency of 193.1 THz and a bandwidth of 50 GHz. This measurement is exactly the measurement of Hong-Ou-Mandel interference [30], in which the visibility shows the indistinguishability between the photons of the two ports. The raw visibility of Hong-Ou-Mandel interference is 84.6 $\pm$ 2.1%, which indicates the generated signal photons and idler photons are well indistinguishable.

The fringes of spatial quantum beating will appear if the signal and idler photons are selected at different frequencies. Fig. 3(b)–(d) are results for one frequency comb pair under different frequency difference between the signal and idler photons ($|\omega_{\mathrm{i}} - \omega_{\mathrm{s}}|$) and filter bandwidth (W), which are adjustable by the pulse shaper. Fig. 3(b) are the results of coincidence counts under the frequency difference of 340 GHz and the bandwidth of 25 GHz. The raw fringe visibility is 81.0 $\pm$ 3.4%. The width of the envelope is about 40 ps and the period of the fringes is about 2.8 ps, which agree with the theoretical calculation according to the frequency difference and bandwidth set by the pulse shaper. When the bandwidth increases to 50 GHz, the measurement results are shown in Fig. 3(c), under the same frequency difference of 340 GHz. It can be seen that the variation of the bandwidth leads to the change of the width of the envelope, which is about 20 ps in this case with similar fringe period (2.9 ps) and raw visibility (81.8 $\pm$ 1.7%) to those in Fig. 3(b). Fig. 3(d) shows the results that the bandwidth is kept to 25 GHz but the frequency difference reduces to 200 GHz. Compared with the results shown in Fig. 3(b), the fringe period increases to 5.0 ps due to the reduction of the frequency difference, while the width of the envelope remains the same and the raw visibility (81.3 $\pm$ 2.1%) is almost unchanged. All the results agree with Eq. (3), indicating that the property of the

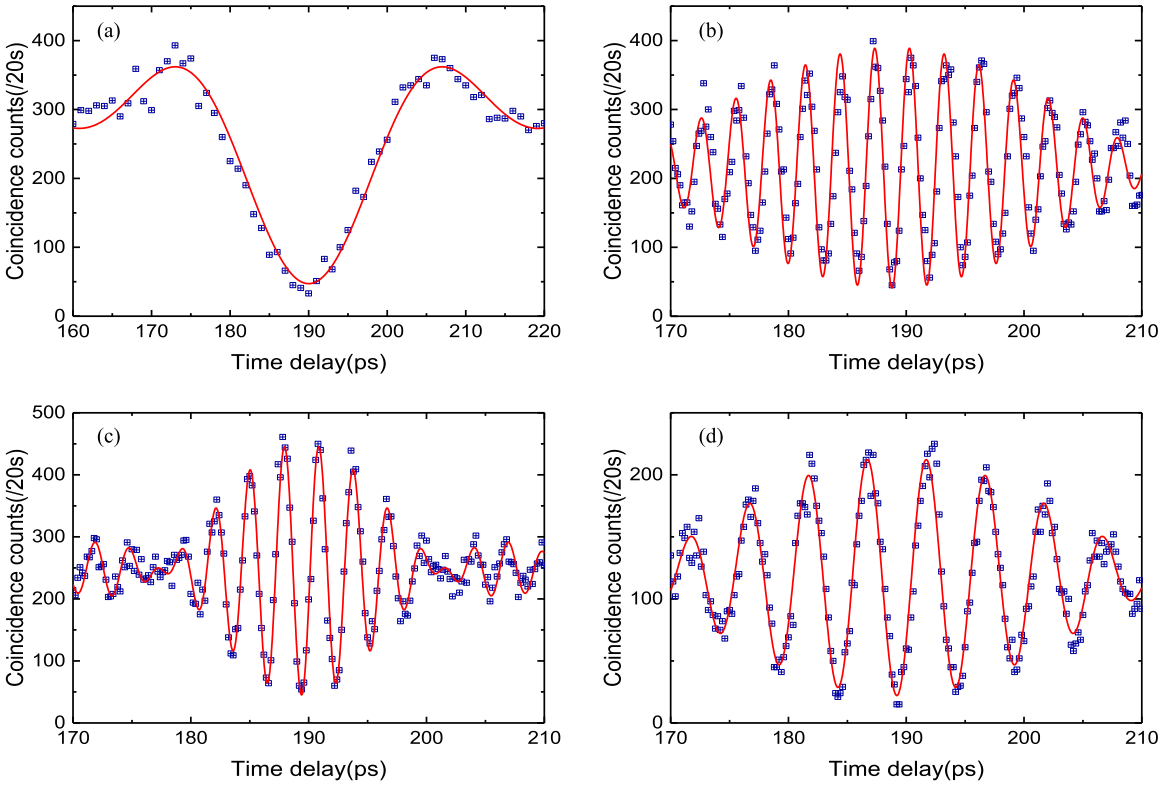

Fig. 3. Results of the spatial quantum beating of one frequency comb pair. (a) The Hong-Ou-Mandel interference for the signal and idler photons with the identical rectangle spectral profile. The raw visibility is 84.6 ± 2.1%. (b)–(d) The fringes of spatial quantum beating for one frequency comb pair under different frequency difference between the signal and idler photons and filter bandwidth. (b) The frequency difference of 340 GHz and the bandwidth of 25 GHz. (c) The frequency difference of 340 GHz and the bandwidth of 50 GHz. (d) The frequency difference of 200 GHz and the bandwidth of 25 GHz. The widths of the envelopes in (b), (c) and (d) are about 40 ps, 20 ps and 40 ps, respectively. The periods of the fringes in (b), (c) and (d) are about 2.8 ps, 2.9 ps and 5.0 ps, respectively. The raw visibilities in (b), (c) and (d) are 81.0 ± 3.4%, 81.8 ± 1.7% and 81.3 ± 2.1%, respectively.

biphoton frequency comb with one comb pair can be flexibly adjusted by the pulse shaper, without impairment on the performance of the biphoton source.

Then, the spatial quantum beating of biphoton frequency comb with N comb pairs is measured. Fig. 4 shows the measured fringes under different biphoton frequency comb parameters adjusted by the pulse shaper. Fig. 4(a) are the results that the comb has 15 frequency components. They form 8 frequency pairs (the two components of the center frequency pair has the same frequency), i.e., $N = 8$. The frequency difference between adjacent components is 25 GHz, and all the frequency components have a rectangle spectral profile with the same bandwidth (W) of 12.5 GHz. It can be seen that the fringes of spatial quantum beating show three dips with a time spacing of 20 ps, and the width of the center dip is about 4.0 ps. It can be considered as a series of dips with an envelope according to Eq. (5). The raw fringe visibility (V in Eq. (5)) is 83.5 ± 5.4%. Fig. 4(b) shows the fringes that the number of the frequency components reduces to seven, while other parameters are kept the same as Fig. 4(a). In this case, the generated comb has four frequency comb pairs, i.e., $N = 4$. It can be seen that the fringes are almost unchanged with a spacing between dips of 20 ps and a raw visibility of 86.1 ± 4.5%, except that the width of the center dip increases to 7.5 ps. Fig. 4(c) shows the results that the frequency difference between adjacent components increases to 50 GHz, while $W = 12.5$ GHz and $N = 4$, the same as Fig. 4(b). It can be seen that the increased frequency difference leads to the decrease of spacing between the dips to 10 ps, and the width of the center dip (4.0 ps) and the measured raw fringe visibility (84.9 ± 3.8%) are almost unchanged.

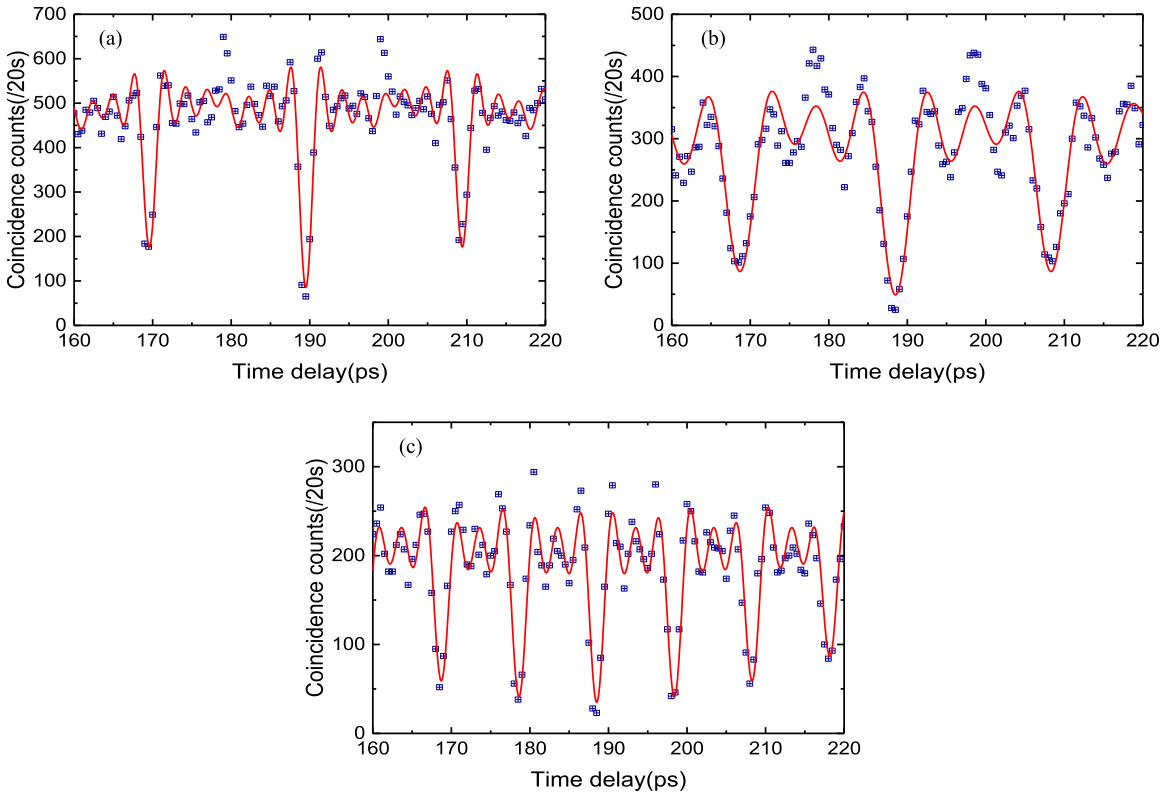

Fig. 4. Results of the spatial quantum beating of N frequency comb pairs under different number of the frequency comb pairs and frequency difference between adjacent components. (a) The same bandwidth of 12.5 GHz and the frequency difference between adjacent components of 25 GHz with 8 frequency comb pairs. (b) The same bandwidth of 12.5 GHz and the frequency difference between adjacent components of 25 GHz with 4 frequency comb pairs. (c) The same bandwidth of 12.5 GHz and the frequency difference between adjacent components of 50 GHz with 4 frequency comb pairs. The time spacings between dips in (a), (b) and (c) are about 20 ps, 20 ps and 10 ps, respectively. The widths of the center dips in (a), (b) and (c) are about 4.0 ps, 7.5 ps and 4.0 ps, respectively. The raw visibilities in (a), (b) and (c) are 83.5 $\pm$ 5.4%, 86.1 $\pm$ 4.5% and 84.9 $\pm$ 3.8%, respectively.

There is a slight discrepancy between the theoretical fitting curve and the experimental data, which may be due to small deviations of the central wavelengths of frequency components in the biphoton frequency comb, since the pulse shaper has a frequency setting accuracy of $\pm$2.5 GHz. Hence, the results of Fig. 4 show that the width of the dips is determined by the whole width of the biphoton frequency comb, and the time spacing between the dips is determined by the frequency difference between adjacent components.

It is worth noting that previous work of biphoton states with multi-frequency comb pairs is usually based on optical resonators [10], [15], in which the adjacent-comb frequency difference is determined by the free space range (FSR) and difficult to change after the physical structure of the resonator is determined. The fringes of spatial quantum beating are usually explained by the interference between the photons output from the resonators after different round-trip time. As a comparison, the frequency-bin entangled biphoton states generated in this work can be controlled by adjusting the setting of the pulse shaper without changing the setup of the source. Since the pulse shaper is based on spatial dispersion components and spatial light modulator [21], the comb-like fringes shown in Fig. 4 cannot be explained by the photon extraction processes of the resonators, however, they still agree with Eq. (5) very well. Moreover, it is noteworthy that the spatial quantum beating measurement cannot reflect phase information between frequency components [31], [32]. The fringes of spatial quantum beating in this work is a signature to reflect different frequency-bin settings of the biphoton frequency comb, however, it cannot be a direct proof of high-dimensional

frequency-bin entanglement. In other words, the spatial quantum beating measurement is a necessary criterion for high-dimensional frequency-bin entanglement.

4. Conclusions

In conclusion, we realize an adjustable biphoton frequency comb and investigate its spatial quantum beating. Vector SFWM processes in a piece of DSF are produced by non-degenerate CW pump lights with orthogonal polarizations to generate broadband biphoton states, and then a pulse shaper is used to realize the biphoton frequency comb with high-dimensional frequency-bin entanglement. Its property could be adjusted by the setting of the pulse shaper. Comb-like fringes with a series of dips are measured in the experiment of spatial quantum beating of biphoton frequency comb with multi-frequency comb pairs. The variations of the beating fringes show the changes of frequency bins in the comb by the setting of the pulse shaper. It can be expected that the adjustable biphoton frequency comb has great potential on high-dimensional quantum information processing and quantum communication based on the frequency degree of freedom.

References

[1] I. Ali-Khan, C. J. Broadbent, and J. C. Howell, "Large-alphabet quantum key distribution using energy-time entangled bipartite states," *Phys. Rev. Lett.*, vol. 98, no. 6, Feb. 2007, Art. no. 060503.

[2] S. Wengerowsky, S. K. Joshi, F. Steinlechner, H. Hübel, and R. Ursin, "An entanglement-based wavelength-multiplexed quantum communication network," *Nature*, vol. 564, no. 7735, pp. 225–228, Dec. 2018.

[3] M. Kues *et al.*, "On-chip generation of high-dimensional entangled quantum states and their coherent control," *Nature*, vol. 546, pp. 622–626, 2017.

[4] M. Krenn, M. Huber, R. Fickler, R. Lapkiewicz, S. Ramelow, and A. Zeilinger, "Generation and confirmation of a (100 x 100)-dimensional entangled quantum system," *Proc. Nat. Acad. Sci.*, vol. 111, no. 17, pp. 6243–6247, Apr. 2014.

[5] T. Giordani *et al.*, "Experimental statistical signature of many-body quantum interference," *Nature Photon.*, vol. 12, no. 3, pp. 173–178, Mar. 2018.

[6] P. Imany, O. D. Odele, J. A. Jaramillo-Villegas, D. E. Leaird, and A. M. Weiner, "Characterization of coherent quantum frequency combs using electro-optic phase modulation," *Phys. Rev. A*, vol. 97, no. 1, Jan. 2018, Art. no. 013813.

[7] P. Imany, O. D. Odele, M. S. Alshaykh, H.-H. Lu, D. E. Leaird, and A. M. Weiner, "Frequency-domain Hong–Ou–Mandel interference with linear optics," *Opt. Lett.*, vol. 43, no. 12, pp. 2760–2763, Jun. 2018.

[8] T. Kobayashi *et al.*, "Frequency-domain Hong–Ou–Mandel interference," *Nature Photon.*, vol. 10, no. 7, pp. 441–444, Jul. 2016.

[9] F. Hudelist, J. Kong, C. Liu, J. Jing, Z. Y. Ou, and W. Zhang, "Quantum metrology with parametric amplifier-based photon correlation interferometers," *Nature Commun.*, vol. 5, no. 1, Dec. 2014, Art. no. 3049.

[10] Z. Xie *et al.*, "Harnessing high-dimensional hyperentanglement through a biphoton frequency comb," *Nature Photon.*, vol. 9, no. 8, pp. 536–542, Aug. 2015.

[11] A. Pasquazi *et al.*, "Micro-combs: A novel generation of optical sources," *Phys. Rep.*, vol. 729, pp. 1–81, Jan. 2018.

[12] M. Kues *et al.*, "Quantum optical microcombs," *Nature Photon.*, vol. 13, no. 3, pp. 170–179, Mar. 2019.

[13] C. Reimer *et al.*, "Generation of multiphoton entangled quantum states by means of integrated frequency combs," *Science*, vol. 351, no. 6278, pp. 1176–1180, Mar. 2016.

[14] L. Olislager *et al.*, "Frequency-bin entangled photons," *Phys. Rev. A*, vol. 82, no. 1, Jul. 2010, Art. no. 013804.

[15] M. Rambach, W. Y. S. Lau, S. Laibacher, V. Tamma, A. G. White, and T. J. Weinhold, "Hectometer revivals of quantum interference," *Phys. Rev. Lett.*, vol. 121, no. 9, Aug. 2018, Art. no. 093603.

[16] Z. Y. Ou and L. Mandel, "Observation of spatial quantum beating with separated photodetectors," *Phys. Rev. Lett.*, vol. 61, no. 1, pp. 54–57, Jul. 1988.

[17] X. Li, L. Yang, X. Ma, L. Cui, Z. Y. Ou, and D. Yu, "All-fiber source of frequency-entangled photon pairs," *Phys. Rev. A*, vol. 79, no. 3, Mar. 2009, Art. no. 033817.

[18] F. Kaneda, H. Suzuki, R. Shimizu, and K. Edamatsu, "Direct generation of frequency-bin entangled photons via two-period quasi-phase-matched parametric downconversion," *Opt. Exp.*, vol. 27, no. 2, pp. 1416–1424, Jan. 2019.

[19] S. Ramelow, L. Ratschbacher, A. Fedrizzi, N. K. Langford, and A. Zeilinger, "Discrete tunable color entanglement," *Phys. Rev. Lett.*, vol. 103, no. 25, Dec. 2009, Art. no. 253601.

[20] A. Fedrizzi, T. Herbst, M. Aspelmeyer, M. Barbieri, T. Jennewein, and A. Zeilinger, "Anti-symmetrization reveals hidden entanglement," *New J. Phys.*, vol. 11, no. 10, Oct. 2009, Art. no. 103052.

[21] A. M. Weiner, "Ultrafast optical pulse shaping: A tutorial review," *Opt. Commun.*, vol. 284, no. 15, pp. 3669–3692, Jul. 2011.

[22] B. Liu and A. M. Weiner, "Space–time focusing in a highly multimode fiber via optical pulse shaping," *Opt. Lett.*, vol. 43, no. 19, pp. 4675–4678, Oct. 2018.

[23] F. Ferdous *et al.*, "Spectral line-by-line pulse shaping of on-chip microresonator frequency combs," *Nature Photon.*, vol. 5, no. 12, pp. 770–776, Dec. 2011.

[24] E. Brainis, "Four-photon scattering in birefringent fibers," *Phys. Rev. A*, vol. 79, no. 2, Feb. 2009, Art. no. 023840.

[25] A. McMillan, Y. P. Huang, B. Bell, A. Clark, P. Kumar, and J. Rarity, "Four-wave mixing in single-mode optical fiber," in *Single-Photon Generation and Detection*. Amsterdam, The Netherlands: Elsevier, 2013, ch. 12.
[26] S. Dong *et al.*, "Generation of hyper-entanglement in polarization/energy-time and discrete-frequency/energy-time in optical fibers," *Sci. Rep.*, vol. 5, no. 1, Aug. 2015, Art. no. 9195.
[27] H. Takesue and K. Inoue, "1.5-μm band quantum-correlated photon pair generation in dispersion-shifted fiber: Suppression of noise photons by cooling fiber," *Opt. Exp.*, vol. 13, no. 20, pp. 7832–7839, 2005.
[28] W. Zhang *et al.*, "NbN superconducting nanowire single photon detector with efficiency over 90% at 1550 nm wavelength operational at compact cryocooler temperature," *Sci. China Phys., Mech. Astron.*, vol. 60, no. 12, Dec. 2017, Art. no. 120314.
[29] S. Dong *et al.*, "Energy-time entanglement generation in optical fibers under CW pumping," *Opt. Exp.*, vol. 22, no. 1, pp. 359–368, Jan. 2014.
[30] C. K. Hong, Z. Y. Ou, and L. Mandel, "Measurement of subpicosecond time intervals between two photons by interference," *Phys. Rev. Lett.*, vol. 59, no. 18, pp. 2044–2046, Nov. 1987.
[31] R.-B. Jin and R. Shimizu, "Extended Wiener–Khinchin theorem for quantum spectral analysis," *Optica*, vol. 5, no. 2, pp. 93–98, Feb. 2018.
[32] N. Lingaraju *et al.*, "Spectral phase coherence in HOM interferometry," in *Proc. Conf. Lasers Electro-Opt.*, San Jose, CA, USA, 2019, paper JTu3A.5.